Hyperspectral imaging of diffracted surface plasmons

Dominic Lepage, Alvaro Jiménez, Dominic Carrier, Jacques Beauvais, and Jan J. Dubowski*

Department of Electrical and Computer Engineering, Interdisciplinary Institute for Innovations in Technology (3IT), Université de Sherbrooke, Sherbrooke, Québec J1K 2R1, Canada
**jan.j.dubowski@usherbrooke.ca*

Abstract: We present the results of far field measurements of the complete 3D dispersion relation of a surface plasmon resonance (SPR) effect induced by an integrated quantum well nanodevice. The light modulations in the far field, where the surface plasmons are extracted by a grating, has been calculated for a continuum of energies and wavevectors injected by the luminescent substrate. We introduce a novel experimental method for direct mapping of the EM wave dispersion that enables the monitoring of massive amounts of light-scattering related information. The quasi-real time method is applied for tracking, in the E(**k**) space, the SPR peak surfaces generated by the investigated nanodevice. Those additional dimensions, measured with scalable tracking precision, reveal anisotropic surficial interactions and provide spectroscopic response for SPR.

OCIS codes: (240.6680) Surface plasmons; (230.0230) Optical devices; (170.4520) Optical confinement and manipulation; (290.0290) Scattering; (120.5820) Scattering measurements.

References and links

1. H. Raether, "Surface-Plasmons on smooth and rough surfaces and on gratings," Springer Tracts Mod. Phys. **111**, 1–133 (1988).
2. R. B. M. Schasfoort, and A. J. Tudos, *Handbook of surface plasmon resonance* (Royal Society of Chemistry, Cambridge, 2008).
3. H. E. de Bruijn, R. P. H. Kooyman, and J. Greve, "Surface plasmon resonance microscopy: improvement of the resolution by rotation of the object," Appl. Opt. **32**(13), 2426–2430 (1993).
4. B. Rothenhäusler, and W. Knoll, "Surface-plasmon microscopy," Nature **332**(6165), 615–617 (1988).
5. D. Lepage, and J. J. Dubowski, "Surface plasmon assisted photoluminescence in GaAs-AlGaAs quantum well microstructures," Appl. Phys. Lett. **91**(16), 163106 (2007).
6. D. Lepage, and J. J. Dubowski, "Surface plasmon effects induced by uncollimated emission of semiconductor microstructures," Opt. Express **17**(12), 10411–10418 (2009).
7. A. Jimenez, D. Lepage, J. Beauvais, and J. J. Dubowski, "Quality of surfaces in the fabrication of monolithic integrated light source SPR system for bio-sensing purposes," Microelectron. Eng. (to be published).
8. A. Giannattasio, and W. L. Barnes, "Direct observation of surface plasmon-polariton dispersion," Opt. Express **13**(2), 428–434 (2005).
9. F. Romanato, K. H. Lee, H. K. Kang, G. Ruffato, and C. C. Wong, "Sensitivity enhancement in grating coupled surface plasmon resonance by azimuthal control," Opt. Express **17**(14), 12145–12154 (2009).
10. P. Arudra, Y. Nguiffo-Podie, E. Frost, and J. J. Dubowski, "Decomposition of Thimerosal and Dynamics of Thiosalicylic Acid Attachment on GaAs(001) Surface Observed with in Situ Photoluminescence," J. Phys. Chem. C **114**, 13657–13662 (2010).
11. C. K. Kim, G. M. Marshall, M. Martin, M. Bisson-Viens, Z. Wasilewski, and J. J. Dubowski, "Formation dynamics of hexadecanethiol self-assembled monolayers on (001) GaAs observed with photoluminescence and Fourier transform infrared spectroscopies," J. Appl. Phys. **106**(8), 083518 (2009).

1. Introduction

The intrinsic surficial sensitivity of the surface plasmon resonance (SPR) effect is a well known consequence of the spatial localization of the electromagnetic fields and charge coupled mode. The surface plasmons (SPs) can be employed as an information carrier to monitor the optical changes occurring within their evanescent field, typically 100 to 200nm

#136059 - $15.00 USD Received 4 Oct 2010; revised 28 Nov 2010; accepted 6 Dec 2010; published 13 Dec 2010

from the metal surface. Multiple commercial and research apparatus exploit the advantageous properties of the SPR for biochemical analysis and imagery of processes localized on metal surfaces.

Conventionally, SPR tracking consists in probing the dispersion relation E(**k**) of the charge coupled electromagnetic (EM) wave under a predetermined condition of resonance in either energy E (fixed incident energy) or in wavevector **k** (fixed incident coupling angle). Time-resolvable biochemical adsorption events can then be monitored for that resonance energy or wavevector [1,2]. The same can be accomplished spatially for a given time using SPR imaging microscopy [3,4]. Tracking of a wavevector (i.e. incidence angle) is more frequently used for its practicality, a consequence of the laser technology capable of delivering collimated and high power beams of monochromatic light. Resonance monitoring in E or k of SPs is often carried out under prism-based Kretschmann–Reather architecture for simplicity and efficiency, but it can result in a complex and bulky experimental setup [1–4].

A more global approach would be to directly monitor the general dispersion relation of any light emitted or diffracted by the architecture, providing a complete map in I(E,**k**) under specific conditions, thus describing the whole system's state. The complete mapping of the dispersion relation of EM signals presents great technological advantages, especially in scenarios where the waves are employed to probe media of various kinds. In the specific case of SPs, their resonance occurs in a particular plane in the tridimensional (3D) space of the intensity distribution of the E(**k**) dispersion. Nonetheless, the measurement of the complete dispersion relation is a complicated experiment because of the fundamental intertwinement of the variables involved. Consequently, the full and simultaneous characterization of EM-waves has so far been impractical because of the difficulty to separate these variables and collect the volume of data that would thus be generated.

We propose a solution to this problem through the use of a hyperspectral imaging technology. The resulting setup can measure and store the dispersion relation properties of any EM waves in quasi real-time with scalable resolution. We have applied this technology to carry out SPR analyses of integrated quantum semiconductor (QS) devices, where the hyperspectral measurements are to be employed for biosensing.

2. SPR induced by uncollimated broadband emissions

The SPR event takes place in the 3D space of the intensity distribution of the dispersion E(**k**). It can be induced optically where an EM wave meets a metal-dielectric interface. At a given energy, E, the resonance is achieved when the projected in-plane wavevector of the incoming EM wave has a wavevector of norm $k_{ll}^2 = k_x^2 + k_y^2 = k_{SPR}^2$, as illustrated in Fig. 1a [1]. This resonance can be met for various energies and values of $\mathbf{k_{SPR}}$, following a SPR dispersion relation $E(k_x, k_y)$ distributed in a 3D Fourier space, as caricatured in Fig. 1b. Following the time-dependent modulations of such SPR surfaces can be employed for high sensitivity spectroscopic tracking of the biochemical events occurring within the SPs evanescent EM fields.

#136059 - $15.00 USD Received 4 Oct 2010; revised 28 Nov 2010; accepted 6 Dec 2010; published 13 Dec 2010

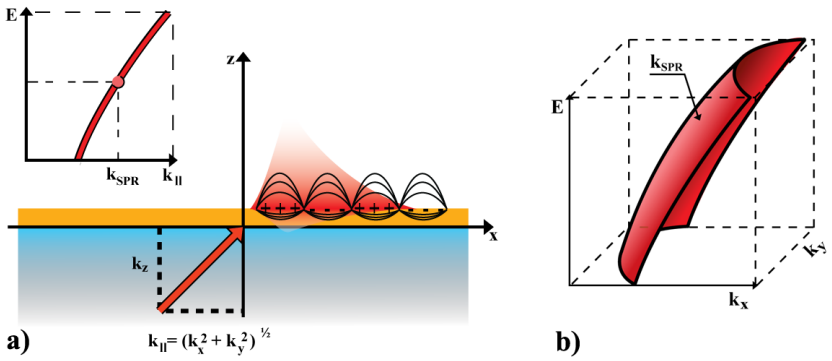

Fig. 1. a) SPR tracking consists in probing the resonance phenomena across the dispersion relation E(**k**) of the charge coupled EM wave under fixed conditions in either energy, E, or in wavevector $\mathbf{k_{II}}$, function of the coupling angles. b) Under specific circumstances, SPR can be induced at any energies where $\mathbf{k_{II}} = \mathbf{k_{SPR}}(E)$. The resulting surfaces in E(**k**) can be employed for high sensitivity spectro-angular SPR tracking.

In a recent publication, we proposed a monolithically integrated SPR microchip design, in which the SPR modes are induced by emissions from an embedded quantum well (QW) nanostructure [5,6]. This was a first step towards a monolithically integrated SPR device, differing from the traditional Kretschmann – Reather configuration. In the proposed design, the SPs are coupled at all possible energies and wavevectors emitted by the substrate light source. As illustrated in Fig. 2 (insert), at any given point of a metallic layer in the dielectric-metal-dielectric (DMD) nanostructure exposed to the whole wavevector spectrum (angles of emission and excitation energies) the coupling will take place for all SPR modes supported by the investigated architecture. While a constant light intensity is measured at a given plane of the real-space, every supported photonic mode is induced at some specific wavevector ($\mathbf{k_{II}}$) emitted by the QW. The observation of the Fourier-space will provide the information about the system's photonic response.

A one-dimensional grating is fabricated atop the metallic layer to diffract the coupled SPs within the measurable light cone at the ± 1st diffraction orders. The architecture of this integrated and self aligned SPR system has also the advantage of coupling two SPR modes, one of which can be used as a signal normalization reference (not shown in Fig. 2) [6]. The signal to noise ratio (S/N) of coupling in the 0th diffraction order was found to increase hundred fold compared to the diffraction assisted SPR coupling. The uncollimated and broadband SPR coupling in such systems implies that the measurement of the dispersion relation of the coupled SPs, traceable in both E and k, would require a highly efficient SPR imaging technique.

The predictions of the far field emissions of the QW-SPR nanostructure are analytically calculated using a tensorial version of Rigorous Coupled-Wave Analysis (RCWA), as depicted before [6]. Any layered architecture could be calculated with multiple parameters, but here we present the results addressing a specific design shown in Fig. 2, where a 20 nm

#136059 - $15.00 USD Received 4 Oct 2010; revised 28 Nov 2010; accepted 6 Dec 2010; published 13 Dec 2010

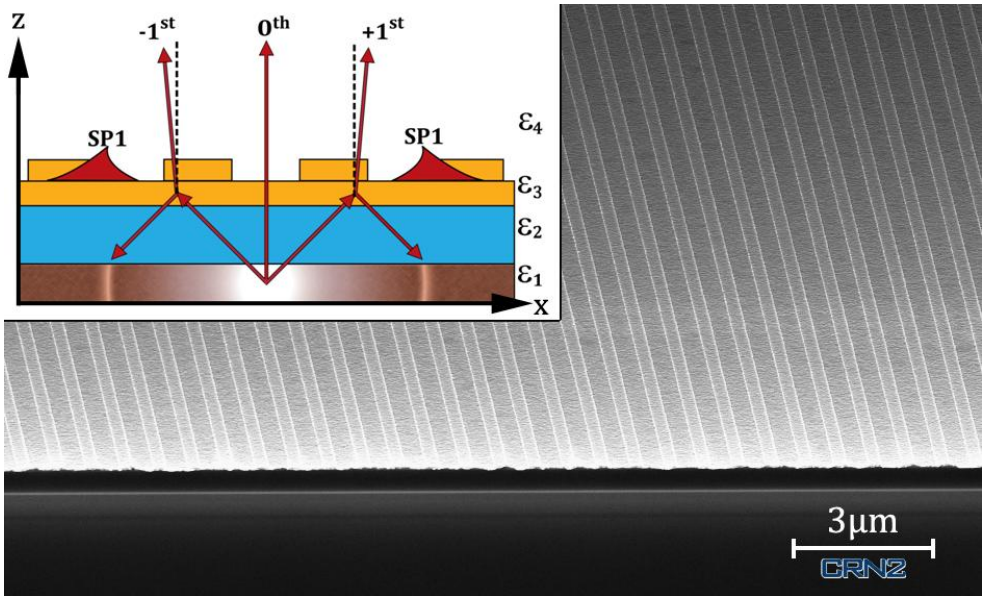

Fig. 2. (*main*) A scanning electron microscope (SEM) image of the architecture comprising an embedded QW structure, an adaptative layer of dielectric and a gold interface with air. (*insert*) The embedded semiconductor (ε_1) emits an uncollimated and usually incoherent light. At a fixed energy, the DMD interface (ε_2 - ε_3 - ε_4) is exposed to a continuous range of wavevector excitations taking place in the Fourier space ($\mathbf{k_{II}}$) and coupling all the photonic modes supported by the architecture. If the light source emits a broad energy spectrum, a continuum of the dispersion relations E($\mathbf{k_{II}}$) can be met.

Au (ε_3) layer is deposited atop 472 nm of SiO_2 (ε_2) on a GaAs-AlGaAs QW structure (ε_1). Atop this structure, we build a 750 nm period Au grating, 20 nm in height and of a ridge to groove ratio of 0.4. The grating covers $1mm^2$ of the substrate and is thus considered quasi infinite since Λ_{SP}<<1mm, where Λ_{SP} is the SPs propagation distance on the surface, calculated at $\mathbf{k_{II}} = \mathbf{k_{SPR}}$ and E = 1.476 eV to be 5.24 ± 0.02 µm ($k_y = 0$). Measurements are carried out in air (ε_4) at room temperature. More details on our fabrication method and various optimization procedures can be found elsewhere [7]. This specific device was designed to couple SPs from the 0th diffraction order for all the energies emitted by its QW microstructure. Diffraction at the ± 1st order occurs on the grating with the SPs propagation through the corrugated grating layer. All the diffraction orders occurring within the structure are taken into account in the calculations, but really become negligible in intensity after the ± 2nd diffraction orders.

Figure 3a presents the predicted k_x-k_y wavevector map in the far field at E = 1.476 eV. Here, the P-polarization (TM) is presented, along with the 0th, ± 1st and ± 2nd diffraction orders. The transmission of the S-polarization (TE) is not shown as it presents no important intensity modulations in **k** and no surficial dependent features. It therefore shifts the intensity modulations by a flat component. The resonance of the SPs is the dominant feature in Fig. 3a,

#136059 - $15.00 USD Received 4 Oct 2010; revised 28 Nov 2010; accepted 6 Dec 2010; published 13 Dec 2010

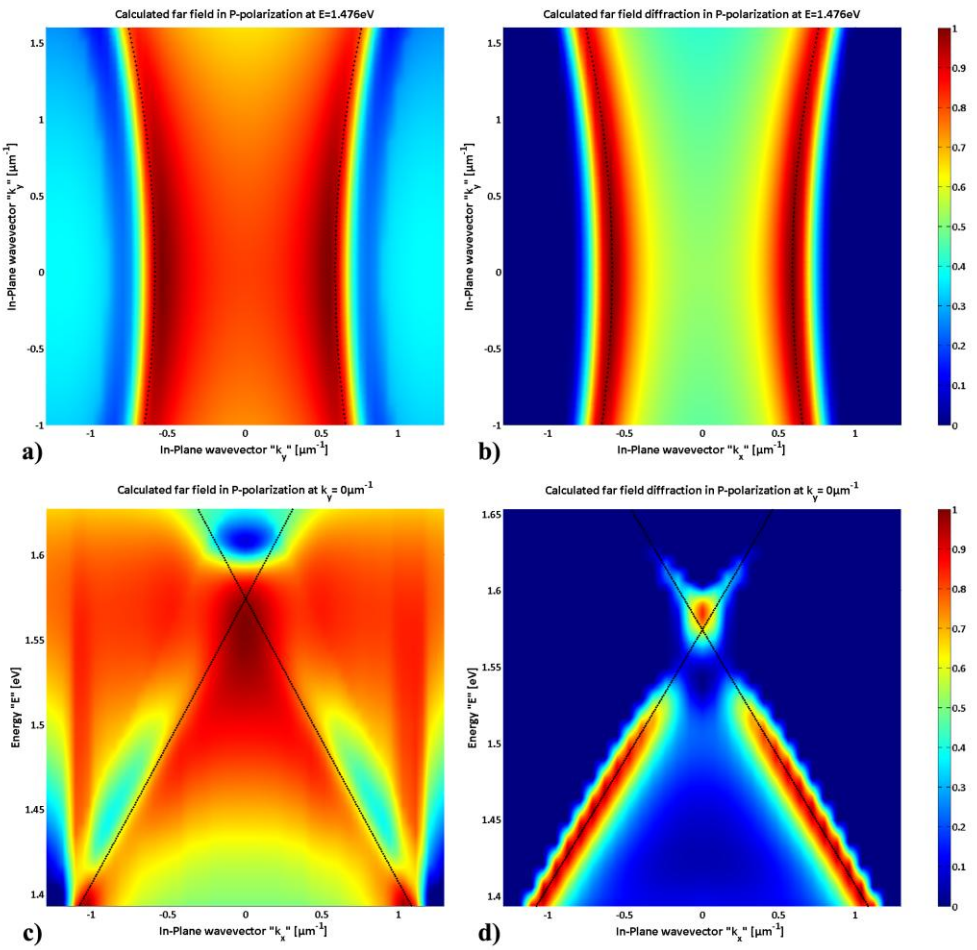

Fig. 3. a) Calculated intensity dispersion in $I(k_x,k_y)$ for the architecture presented in Fig. 2 and a fixed energy of 1.476 eV. The dominant maxima are induced by the in-plane SPs, which are coupled at the 0th order between the Au and air layer, diffracted by the unidimensional grating, as illustrated in Fig. 3b. The black lines are tracking the SPR maxima in **k.** Fig. 3c shows a cross section at $k_y = 0$ of the $I(E, k_x)$, for various energies emitted by the QW structure. Figure 3d illustrates how the main SP features are diffracted in the ± 1st orders. Again, the black lines are following the local maxima from SPR at different energies.

as illustrated in Fig. 3b where only the contribution coming from the ± 1st diffraction orders is shown. The conical diffraction of the one-dimensional grating extract the SPs where $\mathbf{k_{II}} = \mathbf{k}_{SPR} \pm n\,\mathbf{k_G}$, with $n \in \mathbb{Z}$, $\mathbf{k_G} = 2\pi/P\ \hat{x}$, and $|\mathbf{k_x} + \mathbf{k_y}| = |\mathbf{k_{SPR}}|$. Tracking the modulations of the SPR in k_x-k_y space provides a two dimensional surface sensitive method of monitoring biochemical interactions with increased sensitivity [8,9]. The black lines represent the peaks of the diffracted SPs resonance for E = 1.476 eV. Figure 3c now presents a different cut of the calculated far field dispersion $I(E, k_x, k_y)$ emitted by the architecture of Fig. 2, at fixed in-plane wavevector $k_y = 0$. The results are shown for P-polarized light and for all diffraction orders. Again, the main features come from the diffraction in the ± 1st order of the SPR, as isolated in Fig. 3d where only the ± 1st diffraction orders are shown. The modulations in energy (E) from the QW photoluminescence (PL) are not applied for clarity. Here, a projection on $k_y = 0$ of the dispersion relation $E(\mathbf{k})$ of the coupled SPs is visible. The slopes of the lines correspond to the group velocity of SPs propagating in $\pm\ \hat{x}$ directions. Monitoring

#136059 - $15.00 USD Received 4 Oct 2010; revised 28 Nov 2010; accepted 6 Dec 2010; published 13 Dec 2010

the modulations in E(**k**) provides spectral information on surficial events in the SPs near field. The black lines are the local maxima corresponding to diffracted SPs for various E(**k**). One should notice that 2-dimensional projections of light intensities are convenient for demonstration purposes, but the dispersion relations are in fact multidimensional. Thus, the calculations and measurements are actually cubes of light intensities dispersion, where surfaces in $I(E, k_x, k_y)$ represent the SPs state at the architecture's surface. Tracking the time-dependent displacement of those surfaces, as biochemical events take place on the surface of an integrated QW-SPR device, will provide a large amount of data, the equivalent of up to 10^8 traditional SPR experiments carried out concurrently [1,2]. The challenging task to experimentally track the resonance in the $I(E, k_x, k_y)$ space, requires an innovative measuring approach, such as that offered by the hyperspectral imaging technology.

3. Hyperspectral imaging

Hyperspectral imaging technology has been growing in applications for the past decade, where the main fields of interests were found in astronomy, surveillance and crop monitoring. The basic idea is to spectrally (E) spread a 2D map (ex: x-y) into a 3D cube with intensity distribution I(E, x, y). Each resulting pixel of the image now has a full energy spectrum associated with it. We have recently implemented a hyperspectral imaging PL mapping (HI-PLM) instrument to analyze PL of quantum semiconductor microstructures during the functionalization of their surfaces with different molecules [10,11]. Room temperature measurements of I(E, x, y) from up to $1cm^2$ samples could be completed with this instrument in 1 to 10 minutes depending on the spectral and spatial resolution.

We have modified the HI-PLM system to resolve, instead of the x-y space, the wavevectors space k_x-k_y of the light emissions entering the system. The result is a hyperspectral mapping in 3D of the dispersion relation of the emitted light in $I(E, k_x, k_y)$. A specific and direct application of this instrument is the mapping of the dispersion of the light emitted by a quantum semiconductor SPR architecture [5,6], including the diffraction of SPs in energy and wavevectors. Figure 4 presents the basic schematics of the hyperspectral instrument applied for this purpose. The SPR microstructure is placed under a microscope objective (M.O.). The M.O. exit pupil is imaged directly onto a CCD. In the optical path, a real image is formed on the VBG, thus spectrally spreading the wavevector information on the camera. Contrast images in $I(E \cdot k_x, k_y)$ are thus formed for different VBG positions and consequently deconvoluted into hyperspectral cubes of $I(E, k_x, k_y)$.

4. Predicted and measured far field intensities

We employed a Nikon CFI 60 Infinity-Corrected Brightfield M.O. with N.A. = 0.3 that enabled us collecting a range of wavevectors, $\mathbf{k_{//}} = \pm 0.3 \cdot k_0(\mathbf{E})$, with **E** being the set of emitted energies by the QW. The integration of the light intensities are made over the 1 mm^2 grating and the PL of the substrate QW is emitting for a range of energies from 1.38 to 1.65 eV. A hyperspectral cross-section of a wavevector map at fixed E = 1.476 eV is shown in Fig. 5a. The local maxima of this cross-section, corresponding to diffracted SPs, are marked by white dots. The dotted black lines of Figs. 3a and 3b are here superposed. When comparing the features of Fig. 3, we conclude that the distribution in wavevectors of the SPs intensity

#136059 - $15.00 USD Received 4 Oct 2010; revised 28 Nov 2010; accepted 6 Dec 2010; published 13 Dec 2010

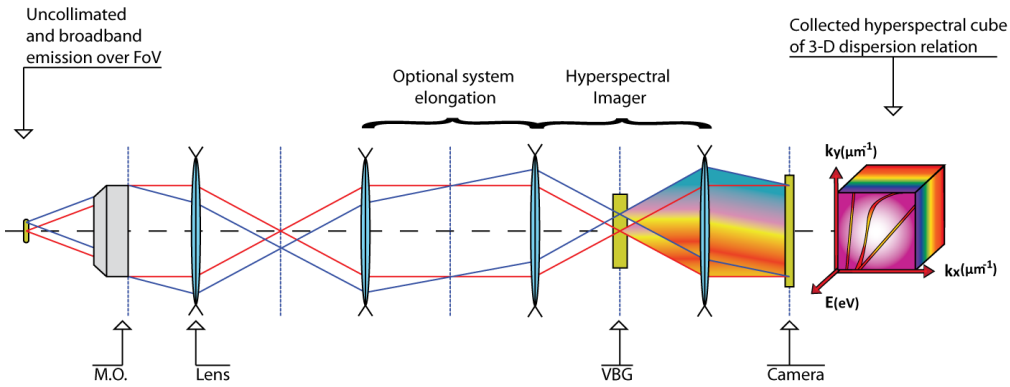

Fig. 4. Hyperspectral setup for mapping of the SPR effect. The integrated SPR microstructure is placed under a microscope objective (MO). The EM emissions from the sample are collimated by the MO and separated spectrally by a volume Bragg grating (VBG). The Fourier plane is then imaged onto a camera. The resulting measurements are 3D cubes of intensities distributed over the emitted energies and collected wavevectors.

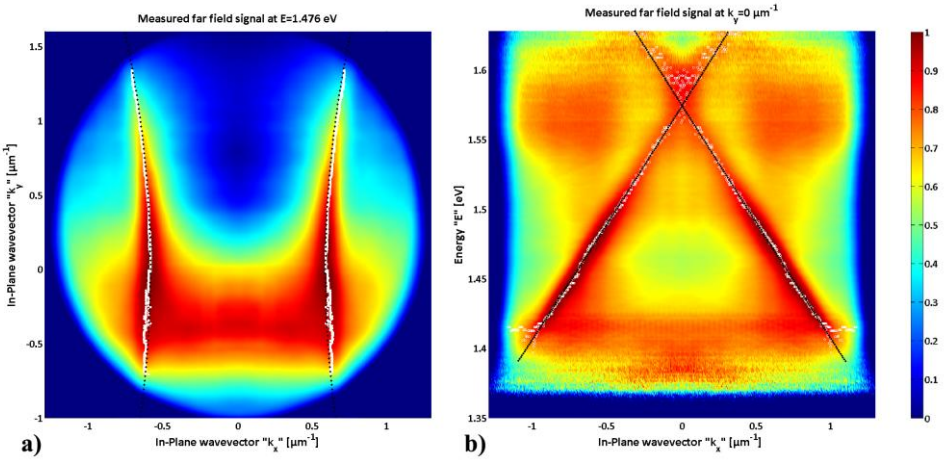

Fig. 5. a) Measured (k_x,k_y) dispersion at 1.476 eV for the architecture presented in Fig. 2. The dominant maxima are induced by the in-plane SPs. The dotted black lines are the analytical SPR peaks shown in Fig. 3 while the white dots are the experimental local maxima. Figure 5b shows another cut at $k_y = 0$ for all the energies emitted by the QW, showing a projected dispersion relation E(k_x). Again, the dotted black lines are the analytical peaks presented in Fig. 3 and the white dots, the experimental local maxima tracking the SPR. Both figures are in very good concordance with the calculations.

reproduces very well with the analytical predictions, where most of the collected signal comes from the diffracted SPs in the ± 1st orders. Also, it can be seen that the positions of the experimental peaks follow those predicted by the calculations. The asymmetric luminescent protuberance, visible around $k_y = 0.35\mu m^{-1}$ for all k_x, was observed for several substrates. We relate it to the misalignment in the hyperspectral system. The second generation system is expected to be free of this problem. Figure 5b presents a different cross-section of the same measurement, this time at $k_y = 0$ for all the energies emitted by the QW microstructure. The local maxima are indicated by white dots and the black lines are those corresponding to the maxima predicted by the analytical calculations of Fig. 3c and 3d. The projected dispersion relation of the device follows the analytical predictions of Fig. 3 very well, with the SPR diffraction as the dominant feature extracted for the far field emission. The signal is normalized for each energy, thus no standard PL curve is visible across Fig. 5, but decreased S/N is seen on the edges where the QW PL is weaker. The peak intensities, corresponding to

#136059 - $15.00 USD Received 4 Oct 2010; revised 28 Nov 2010; accepted 6 Dec 2010; published 13 Dec 2010

SPR, can be tracked and monitored for an energy dependent surface sensing measurement. Within a single measurement, the complete E(**k**) dispersion for SPR can also be extracted in 3D, as shown in Fig. 6. This figure presents the extracted SPR peaks for the whole hyperspectral cube. The two diffracted SPR, from the ± 1st orders, are clearly visible. For the presented cube, each voxel has a resolution of [$0.3 \cdot k_0(\mathbf{E})/1024$ μm^{-1}, $0.3 \cdot k_0(\mathbf{E})/1024$ μm^{-1}, $k_0(\mathbf{E})^2 \cdot c\hbar/2\pi \cdot 10^{-9}$ eV], with cube size [$0.3 \cdot k_0(\mathbf{E})$ μm^{-1}, $0.3 \cdot k_0(\mathbf{E})$ μm^{-1}, **E** eV], with **E** denoting the set of collected energies. It is important to mention that the resolution of the instrument is fully scalable by using different collecting objectives and camera units.

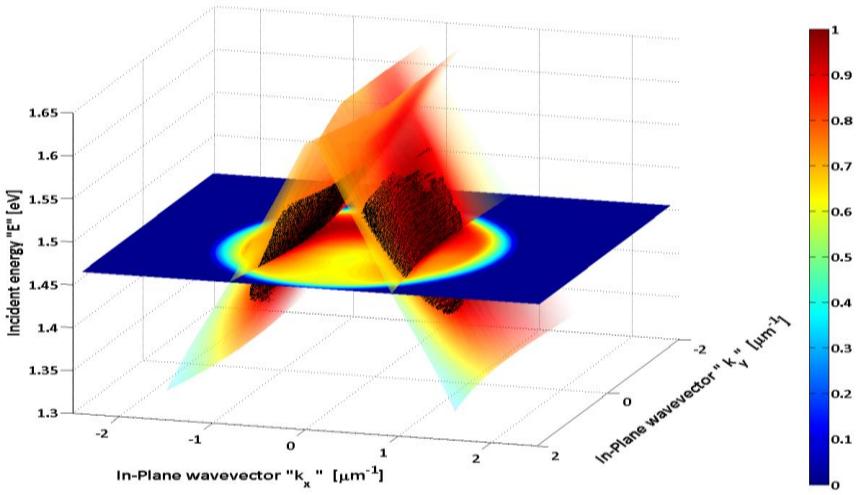

Fig. 6. Measured SPR dispersion in $I(E,k_x,k_y)$ for the integrated architecture presented in Fig. 2. The 3D SPR is extracted from the hyperspectral cube as local maxima, as exemplified by the black dots. The displacement of the 3D SPR in time should provide highly precise spectro-angular information on the biochemical perturbations within the SPs evanescent fields, typically between 100 and 200 nm from the surface.

Measurements reported here were carried out at room temperature and under relatively uncontrolled environmental conditions. It took 15 minutes to collect the cube shown in Fig, 6. This was achieved using a 2x2 binning on the camera and a 1 sec. exposure time for each emitted energy. Faster and more precise measurements could be achieved with a stronger luminescent source that would allow reducing the binning and exposure time. The next challenge will involve the quasi real-time tracking of those SPR dispersion curves, in a 3D space, in order to accurately follow the spectroscopic SPR events taking place on the device surface.

5. Conclusions

SPR on planar metal-dielectric interfaces is a multidimensional phenomenon with a spatially resolvable intensity expressed by $I(E, k_x, k_y)$. The embedment of a broadband light emitter in a substrate of a biosensing architectures allows one to fully take advantage of this phenomenon in a device where many energies are inducing SPR events for a continuum of planar wavevectors.

We have demonstrated the efficiency of tensorial RCWA techniques to predict and optimize such events, especially when a quasi-infinite photonic crystal is involved. The presented case illustrates a 1D metallic grating constructed atop a SiO_2 layer deposited atop a GaAs-AlGaAs QW substrate. The grating allowed the far field extraction of the complete SPs dispersion relation related to the phenomena taking place at the device surface.

To accurately measure the photonic outputs of the proposed integrated GaAs-AlGaAs QW nanodevice, we introduced a hyperspectral measurement method. This enabled us to monitor

#136059 - $15.00 USD Received 4 Oct 2010; revised 28 Nov 2010; accepted 6 Dec 2010; published 13 Dec 2010

the complete dispersion relations of the SPs and presents a novel way of acquiring massive amount of information related to light-scattering and direct mapping of the EM-wave induced phenomena. In the presented case, we showed the particular application for the measurement of SPR and tracking of the peak in a 3D space. The additional dimension of the SPR effect, measured with scalable precision, allows increasing the precision of the tracking, reveals anisotropic surface interactions and provides spectroscopic response of the SPR effect. Our future work will be oriented towards the further improvement of the experimental setup and acquisition methods in order to increase the precision, throughput and ease of access of the instrumentation. Sensitivity calibrations for biochemical agents will also have to be studied.

Acknowledgments

The authors acknowledge the financial contribution from the Natural Science and Engineering Research Council of Canada (NSERC Strategic grant STPGP 350501 - 07), the Vanier Canada Graduate Scholarship (DL) and the Canada Research Chair in Quantum Semiconductors Program (JJD).

#136059 - $15.00 USD Received 4 Oct 2010; revised 28 Nov 2010; accepted 6 Dec 2010; published 13 Dec 2010